IEEE 802.11p VANets: Experimental Evaluation of Packet Inter-Reception Time

M. Elena Renda[a], Giovanni Resta[a], Paolo Santi[a,b], Francesca Martelli[a], and Alessandro Franchini[c]

[a]IIT - CNR, Pisa – Italy

[b]Senseable City Lab, Massachusetts Institute of Technology, Cambridge, MA – US

[c]Tagetik Software, Lucca – Italy

Abstract

Periodic exchange of situational information (beacons) is at the basis of most active safety applications in vehicular environments, which explains recent interest in measurement-based characterization of beaconing performance. However, existing studies are focused on measuring a specific link-level performance parameter, namely, the packet delivery rate (PDR). While PDR is an important performance metric, application requirements of many active safety applications are expressed in terms of the packet inter-reception (PIR) time, whose real-world performance has not been studied so far. In this paper, we fill this gap by presenting an extensive study of the PIR times observed in real-world highway scenarios.

We start by showing that the PIR metric cannot be reliably estimated from PDR, since the two metrics are only weakly correlated. Motivated by this finding, we present a thorough characterization of the PIR time distribution, which is shown to be a power law in a variety of configurations. The shape of the PIR time distribution indicates that potentially dangerous "situational awareness" *blackouts* are relatively frequent. Most importantly, blackout events are found to be directly correlated in time. We also study the effect of vehicle configuration on the PIR time, quantifying the adverse effect of NLOS conditions on the probability of experiencing blackouts. To lessen this effect, we implemented and evaluated, by means of both experiments and simulations, a simple lightweight technique for multi-hop propagation of beaconing information, showing that even relatively simple multi-hop beaconing techniques substantially improve PIR statistics and, hence, safety. A final contribution of this paper is promoting the Gilbert-Elliot model, previously proposed to model bit-error bursts in packet switched networks, as a very accurate model of beacon reception behavior observed in real-world scenarios.

A preliminary version of this paper appeared in the Proceedings of IEEE Infocom, 2012 [19].

Corresponding author: M. Elena Renda (email: elena.renda@iit.cnr.it).

Overall, the wealth of results presented in this paper disclose a number of interesting insights which might prove useful in the design of active safety applications.

Index Terms

Vehicular networks, active safety applications, IEEE 802.11p, beaconing, packet inter-reception time, multi-hop information propagation.

I. Introduction

Vehicular networks are considered a very promising technology to improve safety conditions on the road. Active safety applications are a class of applications enabled by short range vehicular radio communications aimed at raising the level of a driver's "situation awareness", with a substantial benefit in terms of improved safety conditions and better traffic efficiency. Examples of active safety applications are electronic emergency braking light, lane change assistant, lane merging assistant, intersection collision warning, etc. [29].

The successful realization of active safety applications poses hard challenges to the underlying communication technology, which should enable fast and reliable exchange of information between neighboring vehicles in an environment characterized by high mobility and typically harsh radio propagation conditions. The Dedicated Short Range Communication (DSRC) initiative [5] is aimed at defining standards at various levels of the network architecture to realize such dependable short-range radio technology for vehicular communications. In particular, the IEEE 802.11p standard amends the well-known 802.11 protocol suite with the goal of improving quality in vehicular communications. The standard operates in the 5.9 GHz frequency band, and provides data rates between 3 and 27 Mbps.

The fundamental mechanism underlying active safety applications is *beaconing*, through which applications running onboard vehicles become aware of the position and status of surrounding vehicles. Beaconing consists in the periodic broadcast transmission of status messages – called *beacons* – containing vehicle positional and kinematic data. Thus, understanding beaconing performance is a fundamental step in the process of designing active safety applications. This explains the considerable attention that the vehicular networking community has devoted to the study and optimization of beaconing [1], [6], [11], [12], [24], [27], [30], including recent measurement-based studies – see Section II. In particular, two parameters have been identified as the most relevant to characterize beaconing performance: the *beacon delivery rate* and *beacon inter-reception time*.

Beacon delivery rate refers to the fraction of correctly received beacons over the total number of transmitted beacons in a reference time interval, i.e., it is equivalent to the well-known packet delivery rate (PDR) metric. Packet (beacon) inter-reception time (PIR) is defined as the interval of time elapsed between two successful beacon receptions, and is promoted in [6] as a metric that describes the level of "situation-awareness" achieved onboard vehicles more accurately than PDR. To understand why, consider the two following scenarios. In both scenarios, 50% of the beacons transmitted by vehicle A with a 10Hz frequency in an interval of $10\ sec$ are received at vehicle B, i.e., vehicle B receives 50 beacons in both cases. However, the reception pattern is very different. In scenario 1, beacons are received in an alternate fashion: the first beacon is received, the second is missed, the third is received, and so on. In scenario 2, beacons are received in batch: 25 beacons are received in the first 2.5 seconds of the interval, then no beacon is received for $5\ sec$, and the remaining 25 beacons are received in the last 2.5 seconds of the interval. Clearly, scenario 1 and 2 are very different from the situation awareness viewpoint: in the former case, vehicle B's knowledge of vehicle A's position and status is outdated of at most $200\ msec$; in the latter case, there is a situation awareness blackout of at least $5\ sec$. Considering that a vehicle can move of more than one hundred meters in $5\ sec$ at highway speeds, it is clear that situation awareness is severely impaired in scenario 2, resulting in possibly undetected dangerous situations. Thus, monitoring PDR values in the last, say, $10\ sec$ can give only a rough estimate of the level of situation awareness achieved onboard, while the PIR metric is able to deliver a finer grained information. This explains why many active safety applications, such as the class of collision warning applications, mandate requirements in terms of maximum tolerable packet inter-reception time [26].

As reported in Section II, to our best knowledge all existing measurement-based studies of beaconing performance in vehicular networks are focused on PDR evaluation. Thus, what is lacking to date is an understanding of the packet inter-reception times that can be expected in real-world vehicular scenarios. This paper takes a first step towards filling this gap, by presenting an extensive study of the PIR time distribution observed in real-world vehicular links.

The specific contributions of this paper are:

$i)$ *an assessment of the importance of the PIR metric* for estimating the level of onboard "situation awareness". This comes from the observation that *PIR and PDR are weakly correlated metrics*, implying that PDR cannot be used to reliably estimate PIR time;

$ii)$ *a first study of the PIR time distribution observed in highway scenarios*; more specifically, we show

that the *PIR time distribution is heavy-tailed*: it is a power law of relatively low exponent. The *shape* of the PIR time distribution is not affected by vehicle configuration (tall/short), nor by LOS/NLOS conditions, while its *parameters* are. Hence, important metrics such as average PIR time, occurrence of relatively long situation awareness blackouts, etc., are substantially impacted by vehicle configuration.

iii) *a first study of the likelihood of experiencing situation awareness blackouts*; since collision warning application requirements are expressed in terms of a maximum allowed PIR time, estimating the likelihood of experiencing PIR times exceeding the prescribed bound allows understanding to what extent application requirements are met in a real-world scenario. Our study reveals that non only *relatively long situation awareness blackouts are relatively frequent*, but also that *they are likely to occur in batch* since blackout events are positively correlated in time;

iv) *the implementation and evaluation* of a simple, lightweight technique for *multi-hop propagation* of the information reported in beacons. The results of real-world experiments indicate that this technique can be used to significantly reduce the negative effect of NLOS conditions on beaconing performance, and, hence, safety. Furthermore, simulation-based evaluation shows that the benefits of multi-hop propagation of situational information extend beyond the second hop of communication.

Another major contribution of this paper is promoting the Gilbert-Elliot model [7], [9] as a very accurate vehicular link channel model: in the last part of the paper, it is shown that this model, which is renamed L/N model in the context of vehicular networks to emphasize effect of LineOfSight (LOS)/NonLineOfSight (NLOS) conditions on link quality, can be tuned to almost perfectly resemble the beacon reception patterns observed in our collected measurements. Given its simplicity and analytical tractability, the L/N model can be an invaluable tool in the design and analysis of active safety applications.

The rest of this paper is organized as follows. Section II discusses related work. In Section III, the setup of the two measurement campaigns carried out to evaluate beaconing performance is described. Section IV shows that PIR time cannot be reliably estimated using the other beaconing performance metric, namely, PDR. Given this, in Section V we present a measurement-based characterization of the PIR time distribution, and discuss how this distribution is affected by LOS/NLOS conditions and short/tall vehicle configuration. In Section VI, we analyze the probability of observing potentially dangerous situation awareness blackout events, and estimate their expected frequency. Motivated by the observation that NLOS conditions considerably decrease beaconing performance, in Section VII we present the implementation of a simple, lightweight technique for multi-hop propagation of situational information, and evaluate its

performance with both experiments and simulations. In Section VIII, the L/N model of a vehicular link is introduced, and its validity assessed by comparing the PIR time distribution generated by the model with that obtained from measurements. Finally, Section IX draws the conclusions and points to some ideas to further extend the work presented in this paper.

II. Related work

Given its importance within the realm of active safety applications, beaconing performance characterization and optimization has been subject of intensive research in recent years. Most studies are based on analysis and simulation, and are typically aimed at understanding and optimizing the communication parameters (data rate, transmission power, etc.) [12], [27], [28], [30]. In [24], the authors analyze multi-hop information propagation using a simple link model, corresponding to the geometric link model that we will consider in the last part of this paper. Other studies consider specific active safety applications, such as cooperative collision warning [6], [31]. Measurement-based works are present in literature [17], [23], [25], but most of them use, as wireless network interface, different amendements of IEEE standard, like 802.11b [23], [25] or 802.11g [17].

Only very recently some papers have been published reporting results from on-the-field experiments using IEEE 802.11p compliant radios. Here, only results relevant to the beaconing application considered in this paper are discussed, while the several experimental works aimed at evaluating PHY layer features of the vehicular radio link are not considered (see, e.g., [2] and references therein).

To the best of the authors' knowledge, all existing measurement-based studies focus on PDR, and only some of them consider vehicle-to-vehicle communications.

In [11], the authors consider an intersection collision warning application, and evaluate PDR and RSSI as a function of the distance of the two vehicles from the intersection. The authors consider different transmit power values in their study, and conclude that intermediate power levels can provide good performance while at the same time reducing congestion in the wireless channel. In a similar study [18], Mangel et al. evaluates how NLOS conditions impact PDR and RSSI as vehicles approach an intersection. The effects of visibility conditions on channel quality are studied also in [10], where the authors focus on vehicle-to-infrastructure communications.

In [1], the authors present an extensive analysis of PDR in different scenarios for what concerns propagation environment, data rate, etc. The authors also analyze temporal, spatial, and symmetric correlation

of PDR values, and conclude that, while temporal and spatial correlation are weak, symmetric correlation is instead quite strong.

In [20], the authors evaluate the impact of obstructions on vehicular channel quality, which is measured in terms of PDR and RSSI. Building on [20], the authors of [2] propose a radio channel model for wireless simulation accounting for vehicle obstructions.

To the best of the authors' knowledge, none of the existing measurement-based studies addresses the problem of characterizing the PIR time distribution, and its relationship with PDR and other environmental factors such as vehicle configuration. A partial exception is [26], where the authors show the plot of an experimentally derived PIR time cumulative density function which is used to assess the reliability of a forward collision warning application. Our study goes significantly beyond [26] by presenting a characterization of the PIR time distribution in different vehicular links, and by studying the frequency and temporal correlation of potentially dangerous situation awareness blackouts.

Relevant to our work is also the literature on multi-hop information propagation. In [3], the authors present the results of a set of measurements aimed at estimating the effectiveness of two-hop relaying of information, focusing in particular on the effect of short/tall vehicles as relaying node. There are two major differences between our work and [3]. First, in [3] the authors use two antennas on the relaying vehicle to physically separate communication with the front and rear vehicle; on the contrary, in our work the relay vehicle is equipped with a single antenna located in the center of the roof. Second, the authors of [3] *estimate* the PDR observed on the two-hop relaying link by multiplying the PDR values observed in the forward and backward link; on the contrary, in our work we physically implement relaying of situational information, and provides measurements of the *actual* PDR and PIR values observed at the destination vehicle.

III. Experiment setup

A. Hardware configuration

Experiments have been performed using IEEE 802.11p compliant devices, namely the LinkBird-MX v3 units produced by NEC. The LinkBird-MX units are embedded Linux machines (kernel 2.6.19) based on a 64 bits MIPS processor working at 266MHz. The characteristics of LinkBird-MX 802.11p network interface are reported in Table I. LinkBird-MX units were connected to a small-size, omni-directional, $108\ mm$ long WiMo antenna with $5dBi$ gain. The antennas were mounted on the roof of the vehicles in

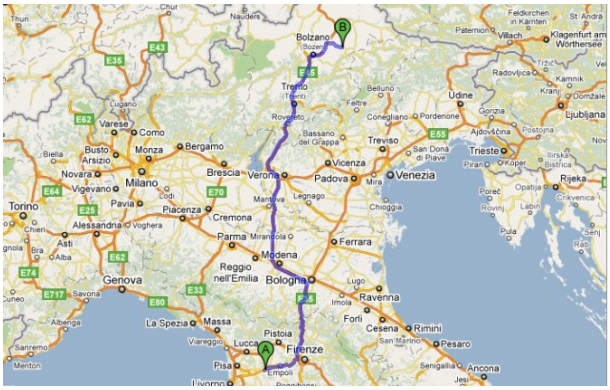

Fig. 1. Map reporting the two-way trip from Montopoli Valdarno to S.Cristina Valgardena (906 Km).

central position as recommended in [13], [18]. The onboard equipment on each vehicle is composed of a LinkBird-MX unit, a GPS receiver, a laptop, and a rooftop antenna. In accordance with European ETSI standard [8], the control channel – channel 180 at 5.9 GHz – has been used for all measurements.

Parameter	**Details**
Frequency/Channel	$5725 - 5925$ MHz
Bandwidth	$10 - 20$ MHz
Version	IEEE802.11p Draft 3.0, July 2007
Transmit Power	Max 21 dBm (Europe)
Bitrates (10MHz)	$3, 4.5, 6, 9, 12, 18, 24, 27$ Mbps
Bitrates (20MHz)	$6, 9, 12, 18, 24, 36, 48, 54$ Mbps

TABLE I
CHARACTERISTICS OF LINKBIRD-MX 802.11P NETWORK INTERFACE.

B. The measurement campaigns

Two measurement campaigns have been carried out to estimate beaconing performance in a highway scenario. In the first measurement campaign, data were collected using *two* vehicles during a two-way trip from Montopoli Valdarno to S. Cristina Valgardena, Italy (see Figure 1) – about $900km$ two-way, and during two two-way trips from Pisa to Florence – see Figure 2 – where each two-way trip is about $176km$. Overall, measurements in this campaign were taken along a total of $1260km$ per vehicle, comprised of about $1151km$ of highways, to which the analysis reported in the following refers.

In the second measurement campaign, data were collected using *three* vehicles during three two-way trips from Pisa to Florence (see Figure 2). Collectively, the measurements collected in this campaign refer to about $500\ Km$ of highway driving per single vehicle.

The reference vehicle configuration used in the second measurement campaign is reported in Figure 3: three vehicles are driven in a typical car-following configuration. Vehicles are named V_0 (head vehicle), V_1 (intermediate vehicle), and V_2 (tail vehicle). Three possible *physical*, IEEE 802.11p links have been

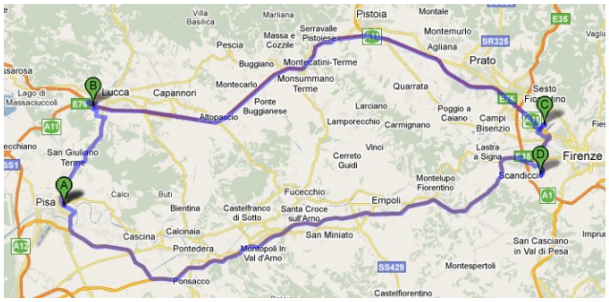

Fig. 2. Map reporting the two-way trip from Pisa to Florence (176 Km).

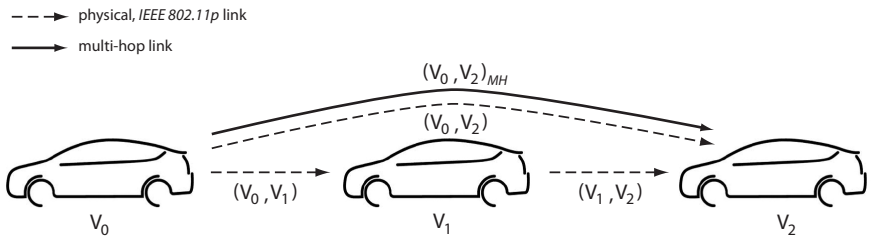

Fig. 3. Reference vehicle configuration for the second measurement campaign.

considered in these measurements: the (directed) links (V_0, V_1), (V_1, V_2), and (V_0, V_2). For the pair of vehicles V_0, V_2, also the *multi-hop* link $(V_0, V_2)_{MH}$ induced by the two-hop information propagation technique described in Section VII is considered, where subscript MH stands for *multi-hop*. The difference between link (V_0, V_2) and $(V_0, V_2)_{MH}$ is that the performance on the former link is measured considering only beacons received at V_2 whose sender vehicle is V_0, while the performance on the latter link is measured considering all beacons received at V_2, including those sent by V_1.

Notice that, although it was not possible to have full control of the vehicle configuration due to the fact that the measurements were conducted in real traffic conditions, the driving goal during the second measurement campaign was to have predominant LOS channel conditions for links (V_0, V_1) and (V_1, V_2), and predominant NLOS channel conditions for link (V_0, V_2). Thus, the results of this measurement campaign can be used also to carefully evaluate the impact of LOS/NLOS conditions on beaconing performance. For the reasons explained above, in the following the term *LOS links* is used to collectively refer to links (V_0, V_1) and (V_1, V_2), and the term *NLOS link* is used to refer to link (V_0, V_2).

In order to investigate the effect of different vehicle configurations on beaconing performance, a different vehicle configuration was used for each of the three trips. In each configuration, there are a tall vehicle (a mini-van, height approx. $1.7m$), and two short vehicles (compact car, height approx. $1.45m$), and the position of the tall vehicle is changed from head, to intermediate, to tail, across the three trips.

C. Performance metrics

Beaconing performance was evaluated according to the following metrics:

- **Packet (beacon) Delivery Rate – PDR**, defined as the ratio between the number of successfully received beacons and the total number of transmitted beacons;
- **Packet (beacon) Inter-Reception Time – PIR**, defined as the time elapsing between the reception of two successive beacons at a specific vehicle; and
- **PIR blackout**, defined as the number and distribution of blackout events, where a blackout is defined as a time interval of length $\geq 1sec$ during which no beacon is received at a specific vehicle.

The length of the time interval used to define a blackout event was empirically set to $1\ sec$, roughly corresponding to the driver's reaction time. The choice of $1\ sec$ as the reference time interval for defining blackouts is also motivated by the observation that a situational-awareness blackout of 1 or more seconds is potentially very dangerous in highway scenarios, where vehicles typically move at a speed of $30\ m/sec$ or higher.

The performance metrics defined above were directly estimated from the recorded measurement logs. The following, additional performance metric is instead *estimated* based on the recorded measurements:

- **blackout frequency**, defined as the average frequency at which blackout events occur. This metric can be estimated from the average PIR time $E(PIR)$ and the PIR blackout probability P_{BO} as follows:

$$BO_{freq} = \frac{P_{BO}}{E(PIR)} \ . \tag{1}$$

  Equation (1) is obtained considering blackout events as independent Bernoulli trials, with success probability $P_{BO} = P(PIR \geq 1\ sec)$, and observing that, on average, PIR events occur every $E(PIR)$ seconds.

The blackout frequency can be considered as an estimate of the actual blackout frequency, due to the fact that, as the results of our measurements have shown, blackout events are time correlated. Disregarding time correlation in equation (1) leads to a slight under-estimation of the actual blackout frequency, quantified in about 7% in a related measurement campaign [15].

IV. Assessing the importance of PIR

As extensively described in Section I, the PIR time is a very important metric for assessing beaconing performance. A first important question to address is the following: *in practical scenarios, can the PIR*

time be reliably estimated starting from PDR, or is it a metric that requires direct measurement? To answer this question, we have used the results of the first measurement campaign to establish whether the two fundamental metrics of beaconing performance, PDR and PIR, are correlated.

We start observing that a sound notion of PIR time requires the vehicles to remain within each other transmission range during the timespan between successive successful beacon receptions. In fact, the aim of the PIR metric is to quantify the degree of situation awareness achieved *when two vehicles are within each other transmission range*. Clearly, there can be no situation awareness if two vehicles are not able to communicate. Hence, we have defined two notions of transmission range based on the measured PDR values as a function of distance, as reported in Figure 4: a *strict* transmission range corresponding to $80m$, and a *loose* transmission range corresponding to $160m$. Once the transmission range is defined, portion of the data traces during which vehicles were not continuously within each other transmission range can be filtered out and not considered in the analysis.

Based on the results of the first measurement campaign, we have computed the Pearson correlation coefficient[1] between PIR time measurement and the PDR observed in the 5 seconds preceding a successful reception event (which corresponds to a PIR time measurement). As seen from Table II, the coefficient reveals a weak inverse correlation between PIR and PDR. Thus, *PDR values cannot be used to estimate PIR time, and PIR time needs direct measurement*. Since relevant PIR events from the situation awareness viewpoint are those corresponding to relatively large PIR values (say, PIR times $\geq 1sec$), correlation coefficient has also been computed on the restricted data set formed of the (PIR, PDR) pairs with $PIR \geq 1\ sec$. As seen from Table II, also in this case correlation is weak, although somewhat stronger than in case the entire data set is considered. Table II shows also the correlation of PIR time with vehicle speed and relative distance, which is reported to be negligible. Notice that the correlation between PIR time and distance is weak because we are analyzing events where vehicles are within each other transmission range, i.e., they are within short distance.

PIR vs.	**All data set**	$PIR \geq 1\ sec$
PDR	-0.2313	-0.3543
distance	0.0856	0.1458
speed	0.0423	0.1084

TABLE II
PEARSON CORRELATION COEFFICIENT BETWEEN PIR TIME AND PDR, DISTANCE, AND SPEED IN THE FIRST MEASUREMENT CAMPAIGN.

[1]The Pearson correlation coefficient takes values in $[-1, 1]$, with -1 and 1 representing maximal correlation (inverse and direct, respectively), and 0 representing no correlation.

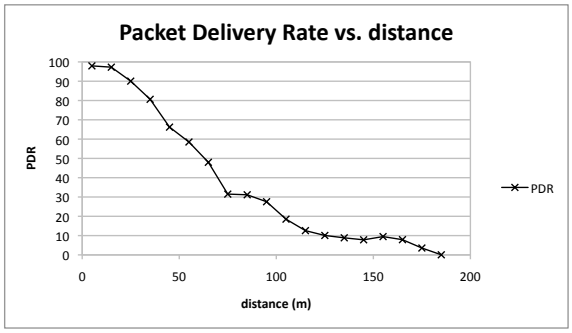

Fig. 4. PDR as a function of distance between vehicles in the first measurement campaign.

V. THE PIR TIME DISTRIBUTION

Motivated by the observation made in Section IV that the PIR metric cannot be estimated from PDR, in this section we characterize the PIR time distribution observed in the experiments.

A first observation that can be derived from the extensive amount of collected data in both campaigns is that the PIR time can be considered, for all practical purposes, as a *discrete* random variable[2]. In fact, PIR values computed from the receiver traces always matched perfectly with a value of the form $k \cdot T$, where $k \geq 1$ is an integer and T is the beaconing period of $100msec$. A relatively more uniform distribution of PIR values in the time line is observed only for the NLOS link in the second measurement campaign, due to the fact that vehicle V_2 can receive beacons from both vehicles V_0 and V_1. Nevertheless, for all practical purposes random variable PIR denoting the time elapsing between two successive successful beacon receptions can be modeled as $PIR = k \cdot T$, where T is a constant corresponding to the beaconing period, and k is a random integer denoting the number of periods elapsed between two successful receptions.

We first analyze the PIR time distributions for strict and loose transmission range resulting from the first measurement campaign, reported in Figure 5. The figure reports the complementary cumulative density function (ccdf) of random variable PIR, i.e., $P(PIR > k)$. The mean value of the PIR random variable is $126.29msec$ with strict transmission range, and $134.92msec$ with loose transmission range. The median is $100msec$ in both cases. Indeed, the PIR distribution is highly concentrated on the first term: event $(PIR = 1)$ has relative frequency 0.9344 with strict transmission range, and 0.9277 with loose transmission range. The remaining probability mass, though, is well spread among the larger terms. In fact, independently of the definition of transmission range, the PIR time ccdf is linear in log-log scale, i.e., *it is a power law*. Indeed, the following power laws fit very well experimental data:

[2]This observation applies to the low channel load scenarios considered in the measurements campaigns.

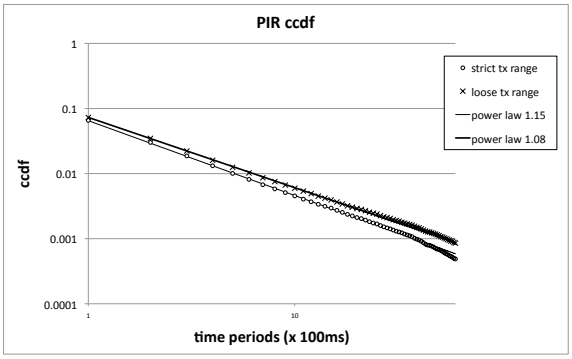

Fig. 5. PIR time ccdf and power law fitting (axes are in log scale) in the first measurement campaign.

$$P(PIR > k) = 0.065 \cdot \left(\frac{1}{k}\right)^{1.15} \quad \text{for strict tx range ,}$$

and

$$P(PIR > k) = 0.073 \cdot \left(\frac{1}{k}\right)^{1.08} \quad \text{for loose tx range ,}$$

We then analyze the PIR time distributions obtained in the second measurement campaign to understand the effects of LOS/NLOS conditions on the PIR time. In this case, based on the observed PDR vs. distance values (not reported due to lack of space), the transmission range is set to $150\ m$. The average PIR time for the three links shown in Figure 3 is reported in Table III, along with the average PIR time obtained in the first measurement campaign. As seen from the table, PIR performance of LOS links is consistent with the measured average PIR time obtained in the first campaign. On the contrary, average PIR time for the NLOS link is considerably higher (up to 100% higher) than that observed in LOS links.

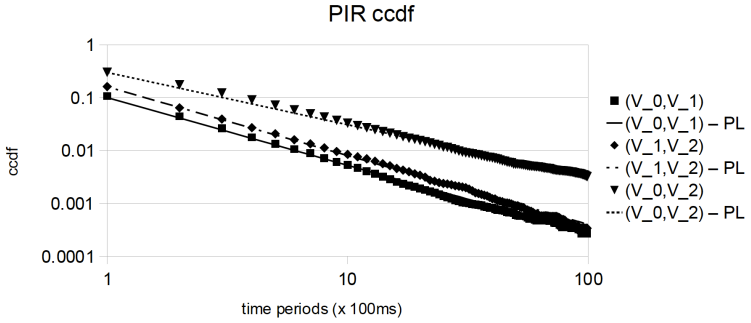

Fig. 6. PIR time ccdf for the three physical links in the second measurement campaign. The figure also reports the power law fits for the three PIR time distributions.

The complementary cumulative density function (ccdf) of the PIR time distribution for the three links is reported in Figure 6. The linear trends in the log-log scale clearly indicate a power law behavior of the

Link	Avg. PIR time	P_{BO}	Blackout freq.	Power Law fit (k, α)
Campaign 1	$135msec$	0.006	$1/22.5sec$	0.073, 1.08
(V_0, V_1)	$133msec$	0.005	$1/26.6sec$	0.1, 1.28
(V_1, V_2)	$150msec$	0.008	$1/18.7sec$	0.16, 1.3
(V_0, V_2)	$267msec$	0.033	$1/8sec$	0.3, 0.99
LOS–TS	$115msec$	0.0003	$1/383sec$	0.18, 1.2
LOS–ST	$109msec$	$4.5 \cdot 10^{-5}$	$1/2422sec$	0.075, 3.15
LOS–SS	$167msec$	0.012	$1/13.9sec$	0.19, 1.25
NLOS–TS	$340msec$	0.058	$1/5.86sec$	0.46, 1.1
NLOS–ST	$173msec$	0.012	$1/14.5sec$	0.24, 1.45
NLOS–SS	$575msec$	0.087	$1/6.6sec$	0.4, 0.65
NLOS–SH	$267msec$	0.033	$1/8sec$	0.3, 0.99
NLOS–MH	$177msec$	0.011	$1/16sec$	0.29, 1.45

TABLE III
PIR TIME CHARACTERISTICS OF THE DIFFERENT VEHICULAR LINKS CONSIDERED IN OUR STUDY, AS PER CONFIGURATION DESCRIBED IN FIGURE 3.

PIR time ccdf for the three links, which is in accordance with what observed in the first measurement campaign. The parameters of the three power laws depicted in Figure 6 are reported in Table III. As seen from the table, the exponent of the power law is very different depending on LOS/NLOS conditions: it is 1.28–1.3 for LOS links, while it is much lower (0.99) for the NLOS link, indicating a much heavier tail of the PIR time distribution.

Next, we analyze the effect short/tall vehicle configuration on the PIR time distribution. We first analyze LOS links, which are further classified as either TS (Tall ahead vehicle and Short following vehicle), ST (Short ahead vehicle and Tall following vehicle), or SS (Short ahead vehicle and Short following vehicle). The average PIR time for the three classes of links is reported in Table III. As seen from the table, *PIR performance is heavily influenced by vehicle configuration*. In particular, comparing ST and SS links, which display best and worst PIR performance, respectively, it can be observed that in SS links the average PIR time is increased of about 53% with respect to ST links. The radically different PIR performance for the SS and ST classes of links is evident also from Figure 7, which reports the PIR time ccdfs. The power law nature of the PIR time distribution is still evident, although the exponent of the power law is very different: it is 1.25 for the SS links and 3.15 for the ST links.

Finally, we analyze the effect of short/tall vehicle configuration on PIR time in the NLOS link. The three possible configurations are called TS, ST, and SS. In TS configuration, the transmitting vehicle is tall, the receiving vehicle is short, and the in-between vehicle is short. The two other configurations are defined similarly.

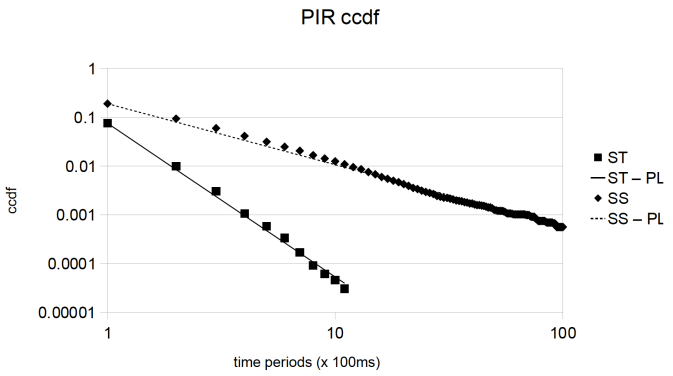

Fig. 7. PIR time ccdf for the SS and ST LOS links in the second measurement campaign. The figure also reports the power law fits for the two PIR time distributions.

The average PIR time for the three classes of NLOS links is reported in Table III. Similarly to the case of LOS links, *PIR performance is profoundly impacted by vehicle configuration*. Comparing performance of ST (best performing) vs. SS (worst performing) link, the average PIR time in the best configuration is about three times lower than in the worst configuration. Notice that in the SS configuration the in-between vehicle is tall, while in the two other configurations the in-between vehicle is short. Thus, the notable difference in performance between SS and ST configuration is likely to be due to the exacerbated NLOS conditions in SS configuration.

The PIR time ccdfs for the SS and ST NLOS links are reported in Figure 8. The plots clearly indicate a much heavier tail of the PIR time distribution for the SS link. It is also interesting to observe that while the PIR time distribution behaves like a power law for the SS link, the power law fit is less accurate in reproducing the behavior of the ST link.

The better link quality in TS and ST configurations is likely due to the fact that, when transmission occurs between vehicles of different heights, the portion of the vehicle roofs in the Fresnel zone is *less* than in the case of vehicles with similar heights – see Figure 9. In fact, it is known that a more obstructed environment in the Fresnel zone tends to decrease signal quality at the receiver [22].

To summarize, we can conclude that the PIR time distribution can be well approximated by a power law in all the considered vehicular links. However, as reported in Table III the parameters of the distribution are heavily dependent on LOS/NLOS conditions and short/tall vehicle configuration. In particular, it is interesting to notice that a significant effect of short/tall vehicle configuration is observed despite the relatively modest difference in height between the short and tall vehicles (approximately $0.3\ m$), which is much smaller than the height difference of $1\ m$ observed in related work [3].

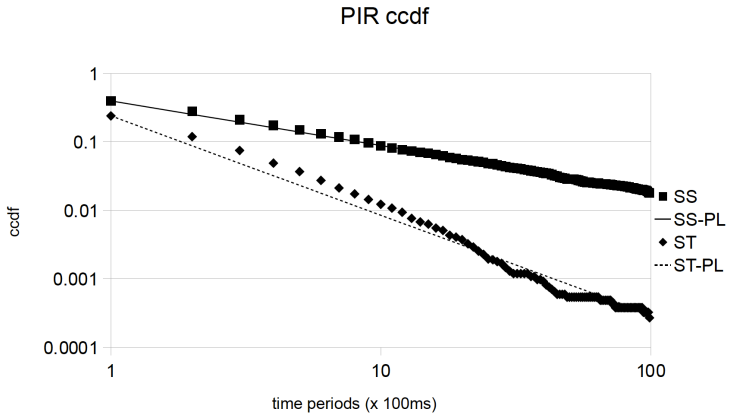

Fig. 8. PIR time ccdf for the SS and ST NLOS links in the second measurement campaign. The figure also reports the power law fits for the two PIR time distributions.

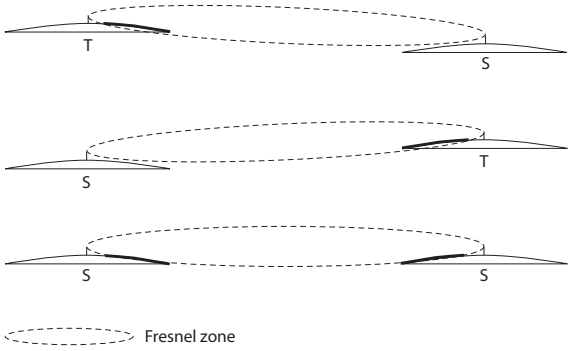

Fig. 9. Fresnel zones for TS (top), ST (middle), and SS (bottom) links. The portion of vehicle roofs in the Fresnel zone is in bold.

VI. Estimating blackout probability

The most important implication of the power law trend observed in Section V is that *the PIR time distribution is heavy tailed*: the probability of having relatively long PIR time is relatively high. Hence, when designing active safety applications, relatively long periods of time during which situation awareness is impaired should be expected.

In this section, based on the collected measurement results we analyze the probability of observing a blackout event, and use this probability to provide an estimate of the expected blackout frequency. We recall that a blackout event is defined as a time interval of length $\geq 1\ sec$ during which no beacon is received. The probability of observing a blackout can then be readily derived from the measured PIR time distribution as[3]

$$P_{BO} = Prob(PIR \geq 10)\ .$$

[3]Recall that random variable PIR is defined as a multiple of the $100ms$ beaconing period.

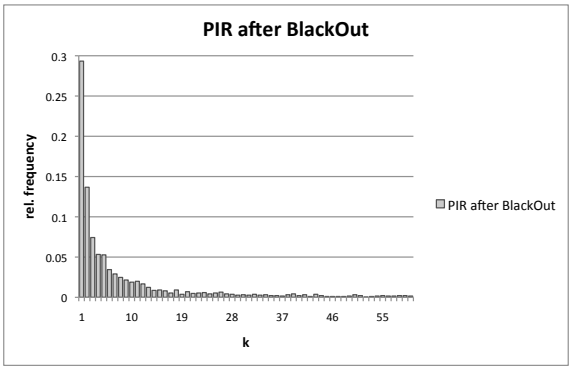

Fig. 10. Probability mass function of the PIR distribution after a blackout in the first measurement campaign.

For instance, the probability of observing a blackout event during the first measurement campaign is about 0.006 with loose transmission range, which is apparently a low value. However, it should be considered that the PIR time value is sampled very frequently: on the average, a new PIR value is generated every $134.92msec$ (loose transmission range). Thus, the average frequency of blackout events can be estimated as

$$BO_{freq} = \frac{P_{BO}}{E(PIR)} = \frac{0.006}{0.13492} \approx \frac{1}{22.5\ sec}\ .$$

Thus, a situation awareness blackout of at least $1sec$ is expected once every $22.5sec$ on average. Considering that a vehicle can easily travel for 30-$40m$ in a highway scenario during $1sec$, it is evident that potentially dangerous situations might remain undetected during blackouts.

The blackout probability observed in the two measurement campaigns are reported in Table III, along with the estimated corresponding blackout frequencies. The notable effect of LOS/NLOS conditions on blackout probability and frequency is evident from the values reported in the table. For instance, the blackout probability in the NLOS link is up to 6 times higher with respect to the LOS links, *indicating a much higher frequency of potentially dangerous situational awareness blackouts in NLOS conditions*. Also short/tall vehicle configuration affects the blackout probability: referring to LOS links and comparing ST and SS links which display best and worst PIR performance, we observe that the blackout probability is increased of over 700 times.

Next, we investigate whether blackout events occur independently or they show some temporal dependence. To answer this question, we have analyzed the results of the first measurement campaign, and evaluated the distribution of the first PIR event after a blackout occurs in case of loose transmission range. More formally, the evaluated quantity is the probability mass function of the conditioned event $(PIR_t = k|PIR_{t-1} > 10)$, where PIR_t is the t-th packet inter-reception time observation. The rationale

for this investigation is the following: if blackouts were temporally independent events, the shape of the PIR distribution obtained conditioning on event $PIR_{t-1} > 10$ would be very similar to the shape of the unconditioned PIR distribution. Otherwise, positive or negative temporal correlation of blackouts is displayed.

The PIR time distribution observed after a blackout is reported in Figure 10. The shape of the distribution is considerably different from that of the unconditioned PIR time distribution (see also Figure 20 later on in the paper): the probability mass of the first event is 0.2933, as compared to 0.9277 in the unconditioned distribution; the mean and median are $1.384sec$ and $250msec$, as compared to $134.9msec$ and $100msec$ in the unconditioned distribution. In general, the probability mass is shifted towards larger terms (heavier tail) in the conditioned distribution. This is reflected in the blackout probability, which is 0.006 in the unconditioned distribution, and it is 0.261 after conditioning, i.e., more than 44 times larger. This clearly indicates a strong positive temporal correlation between blackout events: the fact that a blackout is just occurred considerably increases the probability of observing another blackout in the next sample. Thus, *blackout events are likely to occur in batch*, further challenging the design of effective active safety applications.

Temporal correlation of blackout events can be explained by the strong influence of LOS conditions on the vehicular link quality: if a blackout occurred, it is likely that the link between the two vehicles is in NLOS conditions; if NLOS conditions are relatively persistent, it is then very likely that also the next observed PIR time will be relatively long. This intuition is at the basis of the L/N vehicular link model which will be introduced and assessed against measured data in Section VIII.

VII. Multi-hop beaconing

The results presented in the previous sections have highlighted that NLOS channel conditions significantly decrease beaconing performance, leading to likely unacceptable beaconing performance from an active safety application viewpoint (e.g., an average of 1 blackout event every $8sec$). In this section, we show that multi-hop propagation of the situational information reported in the beacons can significantly alleviate this problem.

A. The multi-hop beaconing application

In order to improve beaconing performance in NLOS conditions, a simple, lightweight technique for multi-hop propagation of situational information has been implemented. The technique is based

on piggybacking situational information of vehicles other than the sender's vehicle in a beacon. This is possible since the standard prescribes a beacon size of approximately $100\ bytes$[4], while sender's vehicle situational information can be encoded in $27\ bytes$ – see Figure 11. Hence, additional situational information can be packed in the beacons without exceeding the recommended size.

Since in a real-world scenario the identity and number of vehicles encountered by a certain vehicle A in, say, the last few seconds changes significantly with time, a *dynamic* data structure should be used by the beaconing application running onboard A to store situational information of surrounding vehicles. For this purpose, the `HashMap` data structure available in Java has been used. This data structure stores `<key,value>` pairs, where `key` is the $vehicleID$, and `value` is a record reporting the situational information of the corresponding vehicle. More specifically, the `value` field reports: $packetID$, $latitude$, $longitude$, $speed$, $heading$, and $GPStime$. The $packetID$ field is used to maintain only up-to-date information in the hash table.

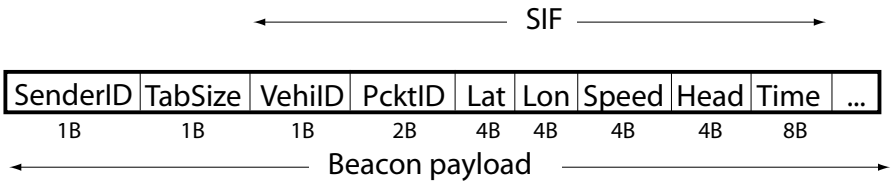

Fig. 11. Beacon format. Situational information is reported using $27bytes$ overall to encode vehicle ID, packet ID, latitude, longitude, speed, heading, and current time.

The beaconing application is composed of a `send` and a `receive` thread. The `send` thread prepares a new beacon and transmits the beacon every $100ms$, i.e., the beaconing frequency is not impacted by multi-hop propagation of situational information. This is in sharp contrast with some existing proposals for beacon-based multi-hop information propagation such as [21], where the beacon transmission time is anticipated/delayed based on the situational information reported in the beacon. While the technique of [21] might prove effective in improving forwarding of situational information of a specific vehicle, it cannot be easily generalized to a scenario like the one considered in this study in which the beacon piggybacks information referring to multiple vehicles. This explains our design choice of keeping the beaconing frequency fixed at $10\ Hz$.

Before preparing the beacon, the `send` thread updates the own information in its own `HashMap` – which contains also the situational information of the sender vehicle –, increasing the $packetID$ value

[4]Excluding the security overhead.

and updating situational information by reading data from GPS. After that, the beacon packet is prepared by introducing a *situational information field* (SIF) for each vehicle in the table – see Figure 11. The beacon payload contains also the ID of the transmitting vehicle ($senderID$), and the number of SIFs reported in the message ($TabSize$). Considering that each SIF is composed of $27\ Bytes$, and that $2\ Bytes$ are needed for the $senderID$ and $TabSize$ fields, the size of beacon payload in the experiments was $83\ Bytes$ – padded to $100\ Bytes$ to comply with recommendations about beacon size [14]. Notice that in the experiment scenario we had three vehicles, hence it was possible to include complete situational information about all involved vehicles in the beacons without exceeding the recommended beacon size. The situation is expected to be different in dense traffic scenarios, where additional techniques shall be used to keep beacon size within acceptable values. For instance, some of the authors of this paper have shown in [16] that network coding can be used to effectively propagate beaconing information in larger vehicle configurations.

The `receive` thread running on vehicle A, upon reception of a beacon sent by vehicle B, checks for each vehicle whether the situational information contained in the beacon is more up-to-date than the one stored in the own `HashMap` table, and if this is the case it updates the corresponding field in the table.

Notice that since both the `send` and `receive` threads can concurrently access the `HashMap` data structure, the `Semaphore` Java class has been used to ensure mutual exclusion. Finally, the `send` and `receive` threads also produce the measurement logs, by recording in a text file each send and receive event.

B. Experimental evaluation

In order to assess the effectiveness of multi-hop information propagation in improving beaconing performance, we use the results collected in the second measurement campaign and compare the performance of the NLOS physical link (V_0, V_2) with that of the corresponding NLOS multi-hop link $(V_0, V_2)_{MH}$. Unless otherwise stated, the results reported in the following refer to the aggregate data collected in the three trips of the second measurement campaign.

The PIR time metrics observed in the two links are reported in the last two rows of Table III. *PIR time performance is very positively affected by two-hop information propagation*: the average PIR time is reduced of about 43% thanks to two-hop information propagation, and the blackout probability is reduced of a factor of 3 with respect to the single-hop NLOS link. The average frequency of blackout events is reduced from 1 event every $8\ sec$ with the single-hop link to 1 event every $16\ sec$ with the multi-hop link. It

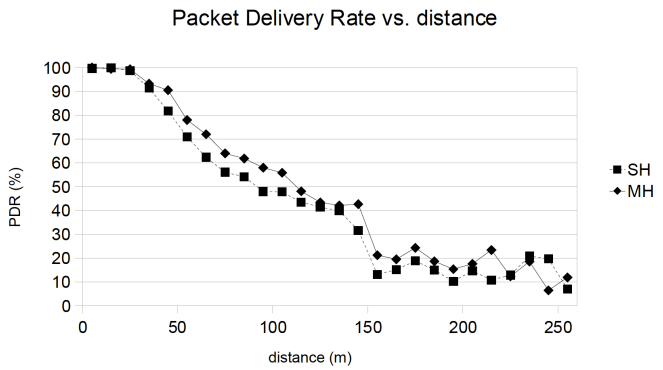

Fig. 12. PDR vs. distance for single- and multi-hop NLOS links in the second measurement campaign.

is interesting to observe that, while PIR performance with two-hop information propagation is considerably improved with respect to the single-hop case, PDR performance improvement is very limited – see Figure 12. This observation confirms the main finding of Section IV, i.e., that PDR beaconing performance is only loosely correlated with PIR performance.

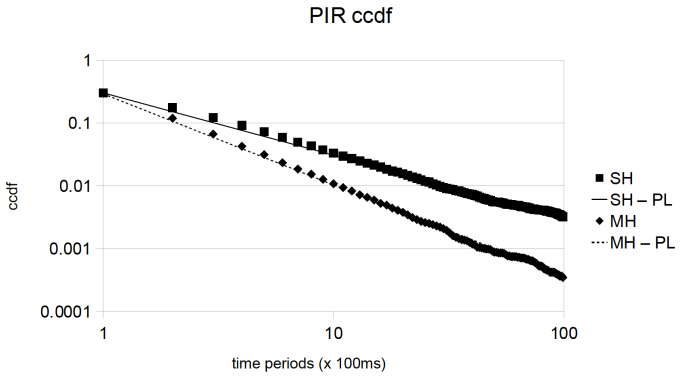

Fig. 13. PIR time ccdf for the single- and multi-hop NLOS links in the second measurement campaign. The figure also reports the power law fits for the two PIR time distributions.

Figure 13 reports the PIR time ccdf of the single- and multi-hop NLOS link. The much heavier tail of the single-hop PIR time distribution can be clearly seen from the plots. It is also interesting to observe that the power law behavior is displayed also by the multi-hop NLOS link. The parameters of the fitted power law curves for the multi-hop link are reported in Table III.

It is interesting to analyze beaconing performance in the most challenging configuration for the NLOS link, namely, the one in which the tall vehicle is in-between two short vehicles. This configuration is interesting since the single-hop NLOS link is in the worst configuration, while the two LOS links that are used to realize two-hop information propagation are in the best (ST) and second-best (TS) configuration – recall the results presented in Section V. Thus, a very noticeable beaconing performance benefit induced by two-hop information propagation is expected with this vehicle configuration.

The analysis of the measurement results fully confirms the above intuition. The PIR beaconing performance in this configuration is reported in Table IV and Figure 14, respectively. The average PIR time with two-hop information propagation is reduced of about 60% with respect to the single-hop link, and the blackout probability is decreased of a factor 4. The resultant average frequency of blackout events is reduced from 1 event every $6.6sec$ in the single-hop link to 1 event every $10.5sec$ in the multi-hop link. It is interesting to observe – Figure 14 – that the multi-hop NLOS link PIR time distribution with short-tall-short vehicle configuration can still be approximated with a power law, although the fit is less accurate than with the single-hop link.

Link	Avg. PIR time	P_{BO}	Blackout freq.	PL fit (k, α)
SH	$575msec$	0.087	$1/6.6\ sec$	0.4, 0.65
MH	$230msec$	0.022	$1/10.5\ sec$	0.39, 1.3

TABLE IV
AVERAGE PIR TIME, BLACKOUT PROBABILITY, AND BLACKOUT FREQUENCY FOR THE SINGLE-HOP (SH) AND MULTI-HOP (MH) NLOS LINK WITH SHORT-TALL-SHORT VEHICLE CONFIGURATION.

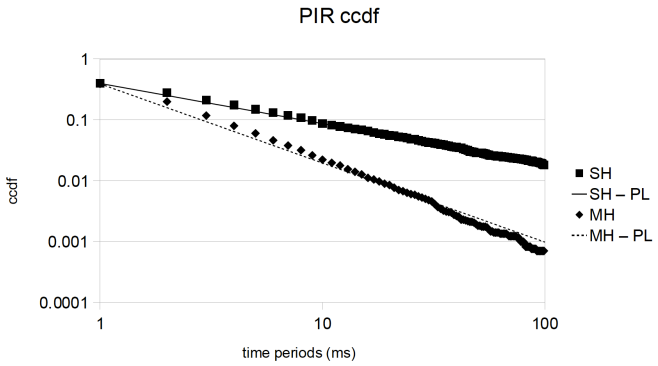

Fig. 14. PIR time ccdf for the single- and multi-hop NLOS links with short-tall-short vehicle configuration in the second measurement campaign. The figure also reports the power law fits for the two PIR time distributions.

C. Simulation-based evaluation

Due to the three vehicle configurations used in the second measurement campaign, the benefits of multi-hop propagation of situational information can be assessed only up to the second communication hop using measurement results. In this section, we resort to simulation to estimate such benefits beyond the second communication hop.

More specifically, the goal of the simulation-based analysis is estimating the time needed for the situational information generated by a vehicle to reach a vehicle located h hops away, with $h = 1, \ldots, 11$.

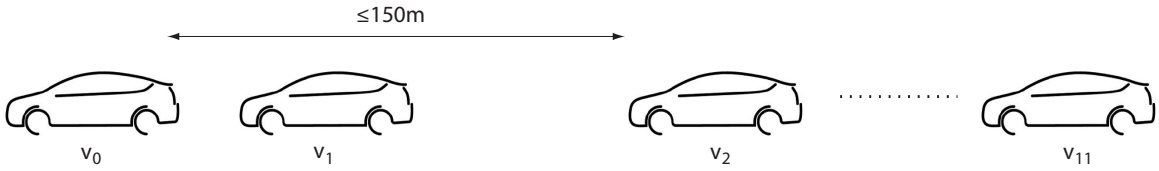

Fig. 15. Reference configuration used in the simulation experiments.

The communication model used to simulate propagation of situational information beyond the second hop is rooted on the findings of the experimental analyses reported in sections V and VII-B. A platoon composed of 12 vehicles is considered, denoted as $v_0, \ldots, v_{11}$ – see Figure 15. Inter-vehicle distances are assumed to be low enough to ensure that the distance between vehicle v_i and v_{i+2} is $\leq 150m$ for any $0 \leq i \leq 9$, to ensure that vehicles at two-hops distance are within each other transmission range – *cfr* Section V. The specific inter-vehicle distance is not relevant as long as the above condition is satisfied, in accordance with the observation made in Section IV that the PIR time is independent of inter-vehicle distance.

Each vehicle in the platoon sends a beacon every $100ms$, including in the beacon the more recent situational data about vehicle v_0 it is aware of. To simulate random access to a non congested channel[5], the order with which beacons are periodically sent is generated uniformly at random, and it is kept unchanged across a single simulation experiment. The beacon sent by vehicle v_i can be received only by vehicle v_{i+1} and v_{i+2}, with beacon inter-reception probabilities governed by the respective one-hop and two-hop PIR time distributions as characterized in Section VII-B. Due to lack of real-world data describing PIR time distribution beyond the second hop of communication, the model used in the simulations considers as zero the probability of receiving a beacon beyond the second hop. This probability, although likely very small, is not zero in a practical scenario. Hence, results reported in the following can be considered as an upper bound to the information propagation time that can be expected in practice.

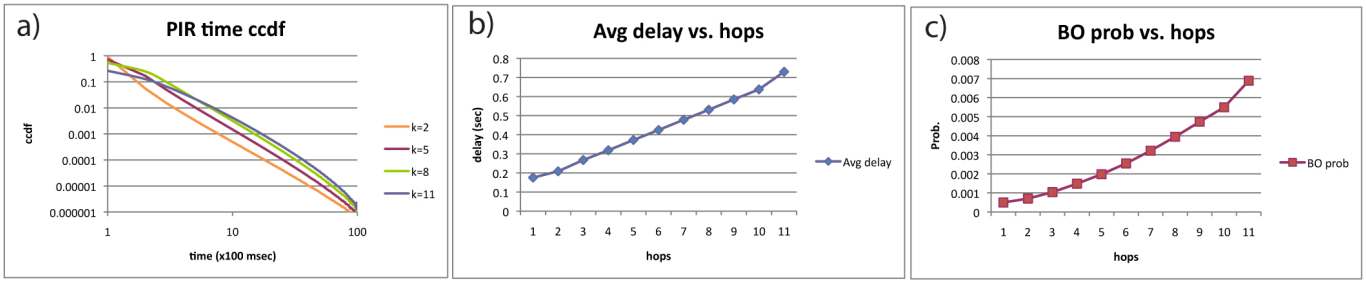

Fig. 16. Results of the simulation-based analysis: PIR time distribution (left), average delay (center), and blackout probability (right).

[5]Twelve beaconing vehicles generate a data load corresponding to about 1.6% of the channel capacity.

The results reported in the following are the average of 10000 simulation experiments, where in a single simulation experiment each vehicle transmits 10000 beacons. Figure 16–a) reports the PIR time distributions observed at 2, 5, 8, and 11 hops from v_0. It is interesting to observe that the PIR time distribution preserves its power law shape also for number h of hops larger than two, the only difference being an increasingly heavier tail with larger values of h. It is interesting to compare the results reported in Figure 16–b) and c), reporting the average information propagation delay and the blackout probability as a function of h, respectively: while the delay displays a linear increasing trend with h, blackout probability displays a super-linear trend with h, reflecting the fact that the tail of the PIR time distribution becomes increasingly heavier with h. This indicates that the probability of experiencing a situational awareness blackout about information generated by vehicle v_0 grows quickly for large values of h. However, the relevance of this information to active safety applications running onboard vehicle v_h quickly *decreases* with h. For vehicles in the immediate surrounding of v_0 – say, up to vehicle v_4 – blackout probability only modestly increases with h, hinting to the fact that multihop propagation of situational information has the potential to substantially benefiting active safety applications.

VIII. VEHICULAR LINK MODELS

In this section we investigate whether a simple vehicular link model resembling observed PIR time distributions can be defined. The answer to this question is obtained by considering three candidate models, which are briefly introduced below. These models are aimed at modeling a situation in which the two vehicles are within each other transmission range, where the transmission range can be thought of as a value empirically defined as in Section V. For simplicity, and in accordance to the observation in Section V, in all models we assume time is discretized into $100\ msec$ steps and model random variable PIR as a *discrete* random variable. In the following, notation $(PIR = k)$ denotes the event "the packet inter reception time equals $k \cdot 100\ msec$".

A. The geometric link model

The geometric model corresponds to the well known model of independent Bernoulli trials, according to which each transmission is successfully received with a fixed probability p. Success probability p is assumed to be independent of the vehicles' speed and relative distance, as long as the two vehicles fall into each other transmission range. When the two vehicles are outside each other transmission range, the reception probability is assumed to be 0. This channel model has been used, e.g., in [24], [31].

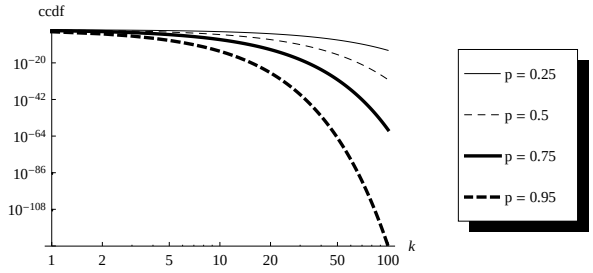

Fig. 17. Ccdf of the PIR time distribution with geometric link model and different values of parameter p.

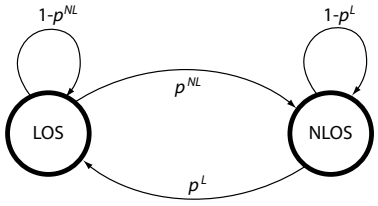

Fig. 18. The L/N link model.

It is straightforward to see that the geometric link model induces a PIR time distribution which is geometric of parameter p, whence the name of the model. In fact:

$$P(PIR = k) = (1-p)^{k-1}p \ ,$$

for $k = 1, 2, \ldots$.

It is also easy to see that the ccdf of the PIR time is:

$$P(PIR > k) = (1-p)^{k} \ .$$

A log-log plot of the PIR time ccdf with geometric link model and different values of p is reported in Figure 17. As seen from the plot, the tail of the PIR time distribution is very thin, unless parameter p is relatively low.

B. The Gilbert model

The Gilbert model has been introduced in [9] to model bit error bursts in packet switched networks. In the Gilbert model, the link can be in two states (GOOD and BAD): when in GOOD state, the bit is correctly received with probability 1; when in BAD state, the bit is correctly received with probability $0 \leq p_{low} < 1$. Transitions between the two states are determined according to transition probabilities p_G and p_B. Thus, the model is fully characterized by three parameters: the link reception probability in BAD

state p_{low}, and the two transition probabilities p_G and p_B.

The PIR time distribution in the Gilbert model can be obtained as a special case of that for the more general Gilbert-Elliot model derived in the next section. Similarly to the geometric link model, the above packet reception probabilities apply only when the two vehicles are within each other transmission range, with reception probability equal to 0 otherwise.

C. The L/N (Gilbert-Elliot) link model

In [7], Elliot introduced a generalization of the Gilbert model in which the probability of correct bit reception in GOOD state is p_{high}, with $p_{low} < p_{high} \leq 1$. The resultant model is known as the Gilbert-Elliot model. The Gilbert-Elliot model is renamed L/N model in this study, motivated by the observation made in Section V that beacon reception probability is heavily influenced by LOS (corresponding to GOOD state) and NLOS (corresponding to BAD state) conditions. The resulting 2×2 Markov chain is pictorially represented in Figure 18. A link can be in either LOS or NLOS state, with transition probabilities p^L, p^{NL} determining the rate of transitions between the two states. The probability of successfully receiving a packet depends on the current link state: it is p_{high}, with $0 < p_{high} < 1$, when the link is in LOS state, and it is p_{low}, with $0 < p_{low} < p_{high}$, when the link is in NLOS state. Note that, given the memorylessness property of a Markov chain, the probability of successfully receiving a beacon at time t depends only on the state of the link at time t, and not on its state at previous time steps. Similarly to the geometric and Gilbert model, the above packet reception probabilities apply only when the two vehicles are within each other transmission range, with reception probability equal to 0 otherwise.

The Gilbert-Elliot model has been mostly used so far to characterize bit-level error burst in a communication, thus the typical quantity of interest has been the number of correctly received bits in a group of m consecutive bits. Conversely, the focus in this study is in characterizing the distribution of two consecutive successful receptions (corresponding to packet, instead of bit, receptions), which, to the authors' best knowledge, has not been studied so far.

The first step in deriving the PIR time distribution in the L/N-model is stating a known property of the two states Markov chain defined above:

Proposition 1 (see, e.g., [4]): If $0 < p^L, p^{NL} < 1$, the unique stationary distribution of the two states Markov chain of Figure 18 is

$$\pi = \left(p_L = \frac{p^L}{p^L + p^{NL}}, \quad p_{NL} = \frac{p^{NL}}{p^L + p^{NL}} \right) .$$

Thus, p_L and $p_{NL} = 1 - p_L$ represent the stationary probabilities of finding the link in state LOS and NLOS, respectively.

Next, the probability $P(L|Rx)$ (respectively, $P(NL|Rx)$) of finding the link in state LOS (respectively, NLOS), conditioned on the event that a beacon has been received, is derived. Probability $P(L|Rx)$ can be computed applying Bayes' theorem:

$$\begin{aligned} P(L|Rx) &= \frac{P(Rx|L) \cdot P(L)}{P(Rx)} = \frac{p_{high} \cdot p_L}{p_L \cdot p_{high} + p_{NL} \cdot p_{low}} = \\ &= \frac{p_{high} \cdot p^L}{p^L \cdot p_{high} + p^{NL} \cdot p_{low}} \end{aligned}$$

and

$$P(NL|Rx) = 1 - P(L|Rx) = \frac{p_{low} \cdot p^{NL}}{p^L \cdot p_{high} + p^{NL} \cdot p_{low}} \ .$$

The value of $P(PIR = k)$, for any $k \geq 1$, can be computed by considering all possible unfolding of the Markov chain during k steps, starting from a reception event. Consider a given k-step unfolding of the Markov chain, i.e. a sequence of k states $S_1, \ldots, S_k$, with $S_i \in \{LOS, NLOS\}$, and let $P(S_1, \ldots, S_k)$ be the probability that the unfolding occurs. The probability that $(PIR = k)$ occurs, conditioned on unfolding $S_1, \ldots, S_k$, can be computed as follows:

$$P(PIR = k|\{S_1, \ldots, S_k\}) = p_{S_k} \cdot \prod_{i=1}^{k-1} (1 - p_{S_i}) \ ,$$

where $p_{S_i} = p_{high}$ if $S_i = LOS$, and $p_{S_i} = p_{low}$ if $S_i = NLOS$.

The probability that unfolding $S_1, \ldots, S_k$ occurs after a reception event can be computed as follows:

$$P(S_1, \ldots, S_k) = P(L|Rx) \cdot \prod_{i=1}^{k} p^{L,S_i} + P(NL|Rx) \cdot \prod_{i=1}^{k} p^{NL,S_i} \ ,$$

where

$$p^{L,S_1} = \begin{cases} 1 - p^{NL} & \text{if } S_1 = LOS \\ p^{NL} & \text{otherwise} \end{cases}$$

and

$$p^{L,S_i} = \begin{cases} 1-p^{NL} & \text{if } S_{i-1} = LOS,\ S_i = LOS \\ p^{NL} & \text{if } S_{i-1} = LOS,\ S_i = NLOS \\ p^{L} & \text{if } S_{i-1} = NLOS,\ S_i = LOS \\ 1-p^{L} & \text{if } S_{i-1} = NLOS,\ S_i = NLOS \end{cases}$$

for $i > 1$. The probabilities p^{NL,S_i} are defined similarly.

Thus, the probability of event $(PIR = k)$ can be computed as follows

$$P(PIR = k) = \sum p_{S_k} \cdot \prod_{i=1}^{k-1} (1 - p_{S_i}) \cdot P(S_1, \ldots, S_k) \ ,$$

where the summation is over all possible k-step unfolding of the Markov chain. Unfortunately, directly computing $P(PIR = k)$ requires summing a number of terms which is exponential in k, which becomes unfeasible for even moderate values of k. However, the $P(PIR = k)$ probabilities can be efficiently computed using the following recursive definition, whose correctness can be formally proved by induction (proof omitted due to lack of space):

$$P(PIR = k) = P(L|Rx)P_{kL} + P(NL|Rx)P_{kN} \ ,$$

where

$$P_{iL} = p^{NL}(1 - p_{low})P_{(i-1)N} + (1 - p^{NL})(1 - p_{high})P_{(i-1)L}$$

$$P_{iN} = (1 - p^{L})(1 - p_{low})P_{(i-1)N} + p^{L}(1 - p_{high})P_{(i-1)L}$$

for $i = 2, \ldots, k$ and

$$P_{1L} = (1 - p^{NL})p_{high} + p^{NL}p_{low}$$

$$P_{1N} = (1 - p^{L})p_{low} + p^{L}p_{high} \ .$$

The ccdf of the PIR time distribution with the L/N link model and different parameter settings is shown in Figure 19. In all the plots reported in the figure, $p_{high} = 0.9$, $p_{low} = 0.1$, and $p^L = p^{NL}$. With these settings, it is easy to see that the probability of successful reception is $p_L \cdot p_{high} + p_{NL} \cdot p_{low} = 0.5$. Different scenarios are considered, modeling a situation where transitions between LOS and NLOS states are relatively frequent ($p^L = p^{NL} = 0.8$ – *unstable* plot), relatively unfrequent ($p^L = p^{NL} = 0.2$ – *stable*

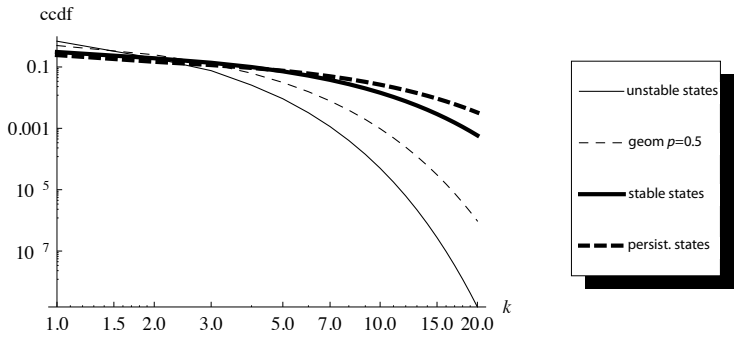

Fig. 19. Ccdf of the PIR time distribution with L/N link model and different parameter settings.

plot), and seldom ($p^L = p^{NL} = 0.1$ – *persistent* plot). For comparison purposes, the plot corresponding to the geometric link model with $p = 0.5$ is also reported. As seen from Figure 19, with the L/N link model the shape of the ccdf varies considerably even if the probability of successful reception is fixed at 0.5. In particular, scenarios with relatively persistent link states result in a fatter tail of the PIR distribution.

D. Validation

In order to assess accuracy of the considered link models in faithfully mimicking beacon reception behavior observed in vehicular links, we have fit all models to the data obtained from first measurement campaign.

Fitting of the geometric model has been done as follows. The expected value of random variable PIR under the geometric link model is $1/p$. Thus, the parameter p of the geometric link model for a specific data set (either strict or loose transmission range) can be computed by setting $p = 1/Avg(PIR)$, where $Avg(PIR)$ corresponds to the average PIR value observed in the first measurement campaign. The resulting values of p are 0.7918 and 0.7411 in the strict and loose transmission range case, respectively.

Fitting of the Gilbert and L/N link model is less straightforward, since the models have three and four parameters, respectively, and the expected value of random variable PIR in these models cannot be readily computed. An iterative search for the best values of the model parameters is then performed, with the goal of minimizing the mean square error (in log scale).

Figure 20 reports the ccdf of the PIR time distribution derived from measurements, as well as the geometric, Gilbert and L/N model fits in case of loose transmission range. Similar results, not reported due to lack of space, have been obtained in case of strict transmission range. From the figure is seen that the geometric link model generates a packet reception behavior that deviates considerably from measured data. The Gilbert model shows a better fit to measurements than the geometric model: however, while it can be

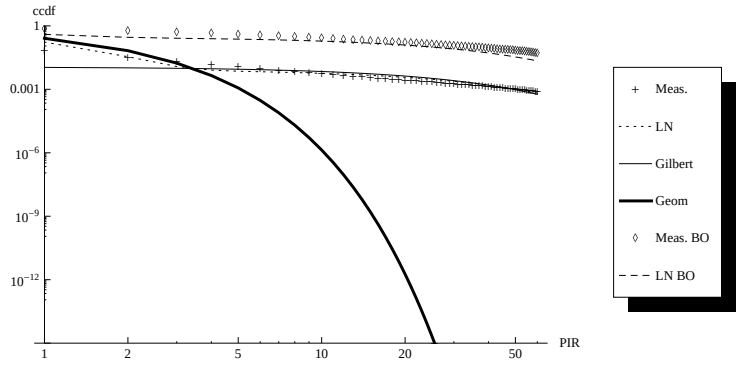

Fig. 20. Measurement-based PIR time ccdf and geometric, Gilbert, and L/N model fittings: unconditioned and conditioned distribution. (Data from the first measurement campaign.)

used to approximate reasonably well the tail of the distribution, it is quite inaccurate in estimating the first terms of the distribution. The L/N model can instead be adjusted to almost perfectly fit experimental data. The resulting best fitting for the L/N model are $p^L = 0.035, p^{NL} = 0.004, p_{high} = 0.825, p_{low} = 0.0125$ in the strict transmission range case, and $p^L = 0.03, p^{NL} = 0.005, p_{high} = 0.835, p_{low} = 0.0125$ in the loose transmission range case. It is interesting to observe that the two best fittings of the L/N model are indeed very similar, indicating that the optimal setting of this model is not very much dependent on the choice of the transmission range.

To further validate accuracy of the L/N-model, the conditional PIR time distribution after a blackout event has been computed, as defined in Section V. The conditional PIR time distribution for the L/N-model has been evaluated by simulating the Markov chain with best fit parameters for 10^6 steps, and recording the observed PIR time after a blackout event. The resulting conditional PIR time distribution is reported in Figure 20, along with that obtained from measurements. As seen from the figure, the L/N-model with best fit parameters as above is able to faithfully reproduce both the unconditioned and conditioned PIR time distribution obtained from measurements. On one hand, this *validates the L/N-model as a simple, analytically tractable, and very accurate vehicular link model*. On the other hand, the fact that L/N-model can be made to almost perfectly fit measured PIR time distribution confirms the observation made from measurements that *the heavily tailed shape of the PIR time distribution is caused by transition between persistent LOS and NLOS conditions, during which reception probability is relatively high and relatively low, respectively*.

IX. Conclusions

This paper reports a first extensive, measurement-based analysis of the temporal beacon reception patterns in vehicular networks. The major findings are that the PIR time distribution is heavily tailed, and that situation awareness blackouts are likely to occur in batch. As discussed in the paper, these findings have important implications on the design of active safety applications, challenging the design of effective solutions.

This study also reveals and quantifies the strong impact of vehicle configuration and LOS/NLOS conditions on beaconing performance. For problematic NLOS links, we implement and evaluate a simple network-level solution: multi-hop information propagation of beaconing information. The results of a measurement campaign, as well as simulation analysis, show the substantial benefits this technique provides in terms of increased safety levels, benefits that extend beyond the second hop of communication. Scalability of the proposed solution to dense traffic scenarios is an open challenge for future work, as discussed in Section VII-A.

Another major contribution of this paper is an empirical proof of the fact that the observed beacon reception patterns are caused by transition between persistent LOS and NLOS link conditions; a byproduct of this proof is the validation of the L/N-model as a simple, analytically tractable, and very accurate vehicular link model, which can be an invaluable tool to assist active safety application designers in the challenge of developing effective solutions.

Finally, it is worth mentioning that an important avenue for future research is studying beaconing performance in presence of radio channel congestion. In fact, back-of-the-envelope calculations show that even in the largest configuration with three vehicles, the load generated by the beaconing applications[6] corresponds to only 0.4% of the available channel bandwidth. An initial study along this line outlines the significant impact of radio channel congestion on beaconing performance [15], hinting to the need of implementing proper congestion control techniques.

References

[1] F. Bai, D.D. Stancil, H. Krishnan, "Toward Understanding Characteristics of Dedicated Short Range Communications (DSRC) From a Perspective of Vehicular Network Engineers", *Proc. ACM Mobicom*, pp. 329–340, 2010.

[2] M Boban, T.T.V. Vinhoza, M. Ferreira, J. Barros, O.K. Tonguz, "Impact of Vehicles as Obstacles in Vehicular Ad Hoc Networks", *IEEE J. Selected Areas in Communications*, Vol. 29, n. 1, pp. 15–28, Jan. 2011.

[3] M. Boban, R. Mereles, J. Barros, P. Steenkiste, O.K. Tonguz, "TVR – Tall Vehicle Relaying in Vehicular Networks", *IEEE Trans. on Mobile Computing*, Vol. 13, n. 5, pp. 1118–1131, 2014.

[6] The load generated by the three beaconing applications equals $30 \cdot 100\ Bytes/sec = 36Kbs$.

[4] A.E.F. Clementi, C. Macci, A. Monti, F. Pasquale, R. Silvestri, "Flooding Time of Edge-Markovian Evolving Graphs", *SIAM Journal of Discrete Mathematics*, Vol. 24, n. 4, pp. 1694–1712, 2010.

[5] "Standard Specification for Telecommunications and Information Exchange Between Roadside and Vehicle Systems - 5Ghz Band Dedicated Short Range Communications (DSRC)", *ASTM E2212-03*, 2003.

[6] T. ElBatt, S.K. Goel, G. Holland, H. Krishnan, J. Parikh, "Cooperative Collision Warning Using Dedicated Short Range Wireless Communications", *Proc. ACM VANET*, pp. 1–9, 2006.

[7] E.O. Elliot, "Estimates of Error Rates for Codes on Burst-Noise Channels", *Bell Syst. Tech. J.*, V. 42, pp. 1977–1997, 1963.

[8] ETSI TC ITS, "Intelligent Transportation Systems (ITS): European Profile Standard on the Physical and Medium Access Layer of 5Ghz ITSs", draft ETSI ES 202 663 V.0.0.6, Oct. 2009.

[9] E.N. Gilbert, "Capacity of Burst-Noise Channel", *Bell Syst. Tech. J.*, Vol. 39, pp, 1253–1265, 1960.

[10] J. Gozalves, M. Sepulcre, R. Bauza, "IEEE 802.11p Vehicle to Infrastructure Communications in Urban Environments", *IEEE Communications Magazine*, Vol. 50, n. 5, pp. 176–183, 2012.

[11] K. Hong, D. Xing, V. Rai, J. Kenney, "Characterization of DSRC Performance as a Function of Transmit Power", *Proc. ACM VANET*, pp. 63–68, 2009.

[12] D. Jiang, Q. Chen, L. Delgrossi, "Optimal Data Rate Selection for Vehicle Safety Communications", *Proc. ACM VANET*, pp. 30–38, 2008.

[13] S. Kaul, K. Ramachandran, P. Shankar, S. Oh, M. Gruteser, I. Seskar, T. Nadeem, "Effect of Antenna Placement and Diversity on Vehicular Network Communications", *Proc. IEEE Secon*, pp. 112–121, 2007.

[14] J.B. Kenney, "Standards and Regulations", in *VANET: Vehicular Applications and Inter-Networking Technologies*, John Wiley and Sons, Chichester, UK, 2009.

[15] F. Librino, M.E. Renda, P. Santi, "Measurement-based Modeling of Packet Inter-Reception Times in Presence of Radio Channel Congestion", *Proc. IEEE Secon*, 2014.

[16] F. Librino, M.E. Renda, P. Santi, "Evaluating Multi-Hop Beaconing Forwarding Strategies for IEEE 802.11p Vehicular Networks", *IEEE Vehicular Networking Conference*, pp. 31-38, 2013.

[17] G. Marfia, M. Roccetti, A. Amoroso, G. Pau, "Safe driving in LA: Report from the greatest intervehicular accident detection test ever", *IEEE Trans. on Vehicular Technology*, Vol. 62, n. 2, pp. 522–535, Feb 2013.

[18] T. Mangel, M. Michl, O. Klemp, H. Hartenstein, "Real-World Measurements of Non-Line-Of-Sight Reception Quality for 5.9Ghz IEEE 802.11p at Intersections", *Proc. Nets4Cars*, pp. 189–202, 2011.

[19] F. Martelli, M.E. Renda, G. Resta, P. Santi, "A Measurement-based Study of Beaconing Performance in IEEE 802.11p Vehicular Networks, *Proc. IEEE Infocom*, pp. 1503–1511, 2012.

[20] R. Meiereles, M. Boban, P. Steenkiste, O. Tonguz, J. Barros, "Experimental Study of the Impact of Vehicular Obstructions in VANETs", *Proc. IEEE Vehicular Networking Conference (VNC)*, pp. 338–345, 2010.

[21] J. Mittag, F. Thomas, J. Harri, H. Hartenstein, "A Comparison of Single- and Multi-Hop Beaconing in VANETs", *Proc. ACM VANET*, pp. 69–78, 2009.

[22] A.F. Molisch, *Wireless Communications*, John Wiley and Sons, Chichester, UK, 2005.

[23] M. Moske, H. Fussler, H. Hartenstein, W. Franz, "Performance measurements of a vehicular ad hoc network", *Proc. IEEE 59th VTC*, pp. 2116–2120, 2004.

[24] G. Resta, P. Santi, J. Simon, "Analysis of Multi-Hop Emergency Message Propagation in Vehicular Ad Hoc Networks", *Proc. ACM MobiHoc*, pp. 140-149, 2007.

[25] J. Santa, M. Tsukada, T. Ernst, A. F. Gomez-Skarmeta, "Experimental analysis of multi-hop routing in vehicular ad-hoc networks", *Proc. 5th Int. Conf. TridentCom Workshops*, pp. 1–8, 2009.

[26] M. Sepulcre, J. Gozalvez, "Experimental Evaluation of Cooperative Active Safety Applications based on V2V Communitcations", *Proc. ACM VANET*, pp. 13–20, 2012.

[27] M. Torrent-Moreno, D. Jiang, H. Hartenstein, "Broadcast Reception Rates and Effects of Priority Access in 802.11-based Vehicular Ad Hoc Networks", *Proc. ACM VANET*, 2004.

[28] H. Venkataraman, A. d'Ussel, T. Corre, C. H. Muntean, G.-M. Muntean, "Performance analysis of real-time multimedia transmission in 802.11p based multihop hybrid vehicular networks", *Proc. 6th Int. Wireless Commun. Mobile Comput. Conf.*, pp. 1151–1155, 2010.

[29] VSC Consortium, "Vehicle Safety Communications Project Task 3 – Final Report: Indentify Intelligent Vehicle Safety Applications Enables by DSRC, *DOT HS 809 859*, March 2005.

[30] K. W. Wolterink, G. J. Heijenk, G. Karagiannis, "Information dissemination in VANETS by piggybacking on beacons - An analysis of the impact of network parameters", *Proc. IEEE Vehicular Networking Conference*, pp. 94–101, 2011.

[31] X. Yang, J. Liu, F. Zhao, N.H. Vaidya, "A Vehicle-to-Vehicle Communication Protocol for Cooperative Collision Warning", *Proc. IEEE MobiQuitous*, pp. 1–10, 2004.